

Ground System Phase Estimation Techniques for Uplink Array Applications

L. Paal,¹ R. Mukai,² V. Vilnrotter,² T. Cornish,¹ and D. Lee²

Phase drift in the radio frequency (RF) signals distributed to individual antennas of an uplink array degrades the array phase calibration vector, resulting in loss of combined power at the spacecraft. Since the calibration vector generally is not applied to the uplink array right after calibration, small changes in the electrical characteristics of the ground distribution system over time could result in significant changes in phase, which must be measured and removed in order to preserve the integrity of the calibration vector. This article describes practical techniques for determining the electrical length of the fiber-optic distribution system in real time, and applies these measurements to estimate unwanted changes in RF phase that could impact uplink array operation if left uncorrected.

I. Introduction

A real-time technique for measuring the effective electrical distance to the array antennas is presented in this article, together with techniques for determining the time-varying phase at each antenna due to thermal effects and equipment drift on the ground. Since the carriers at each antenna accrue different Doppler frequencies due to array geometry, which in turn impacts the phase estimation algorithms, a method for removing the time-varying Doppler is discussed. A detailed mathematical model of the uplink array ground system is developed, algorithms for estimating phase drifts are defined, and some preliminary experimental results carried out using existing equipment at Signal Processing Center 10 (SPC 10) are presented.

One of the difficulties in determining the appropriate uplink phase vector is compensating for phase differences present among the antennas on the ground. In general, the exact electrical distance, defined here as the effective signal propagation distance from the control center to the antenna, is not precisely known. This results in unknown phase differences among the antennas in an array. Furthermore, thermal effects and equipment changes result in changes in the effective electrical distance seen by the central array controller. Additionally, since the antennas in an array are at different spatial locations, the frequency predicts for each antenna generally differ to a certain extent, particularly if the antennas are far apart, since the Doppler for each antenna with respect to a given spacecraft may change significantly depending on the antenna's geographical location. All of these issues result in the presence of unknown, time-

¹ Communications Ground Systems Section.

² Communications Architectures and Research Section.

The research described in this publication was carried out by the Jet Propulsion Laboratory, California Institute of Technology, under a contract with the National Aeronautics and Space Administration.

varying phases among the ground antennas. These time-varying phases must be accurately measured and compensated if coherent combining of the array carriers at the spacecraft is to be successful.

II. Round-Trip Measurement of Electrical Phase

We begin by developing a model of the uplink array ground system and defining the key ideas in round-trip electrical distance measurement. As shown in Fig. 1, the ground system consists of the 7.15-GHz (X-band) exciters at SPC 10, X-band couplers and a round-trip phase comparator assembly at SPC 10, optical fibers for signal distribution to the transmitting antennas, X-band couplers at the output of the power amplifiers at each antenna, and additional optical fibers to return the coupled signal samples to SPC 10 for comparison. The two-way optical-fiber distribution network to and from the antennas is located in the same bundle for most of the approximately 16-km distance from SPC 10 to the Apollo cluster, resulting in similar thermal behavior for the outgoing and returning signals. At the Apollo station, the individual fibers are broken out from the common bundle and routed to their respective antennas, typically a distance of a few hundred meters, over which the fibers may experience independent thermal environments.

A small fraction of the amplified X-band signal is coupled at the output of the transmitter power amplifier (PA) and routed back to SPC 10, where the phase of the signal is compared to that of the transmitted phase, using the real-time phase comparator assembly (PCA) shown in Figs. 2(a) and 2(b). Since the transmitted signal serves as reference for the return signal, the reference distribution system need not be used to establish and maintain the local oscillator (LO) frequency, which is needed for the complex downconversion operation. The inputs to the PCA are the outgoing (reference) and return (sample)

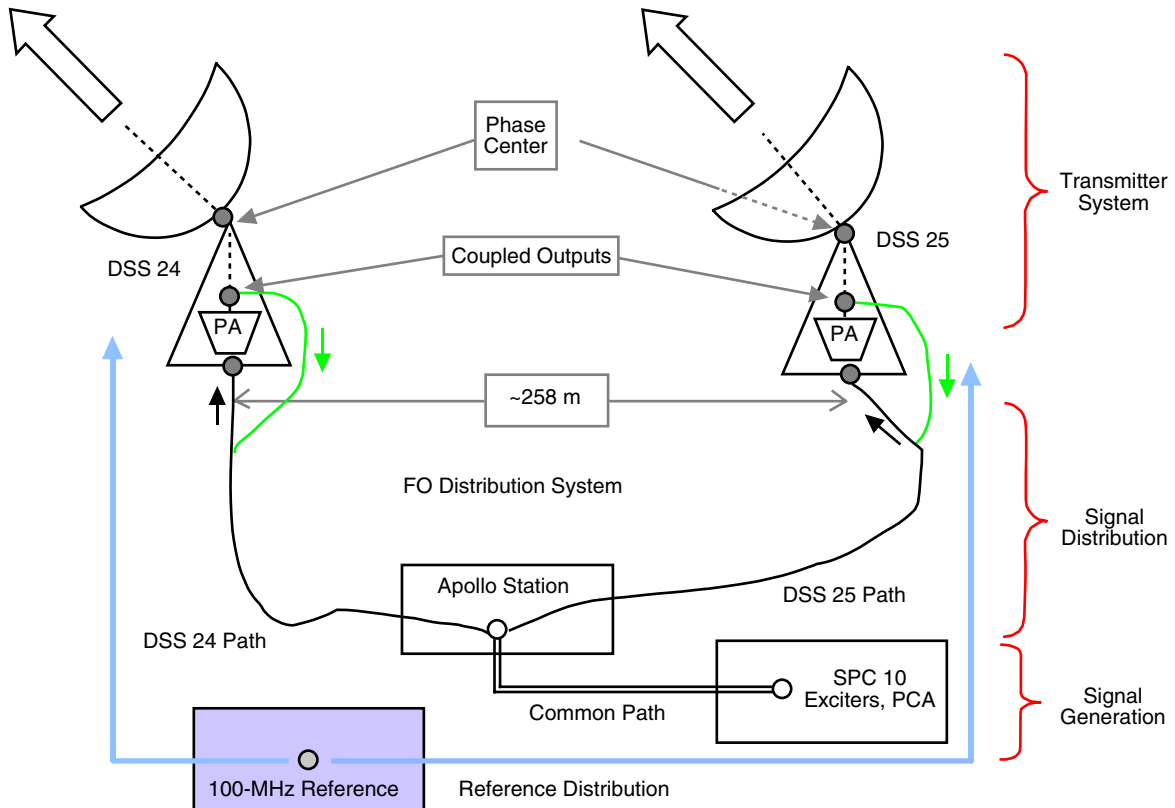


Fig. 1. Block diagram of the signal generation and distribution system from SPC 10 to the Apollo complex.

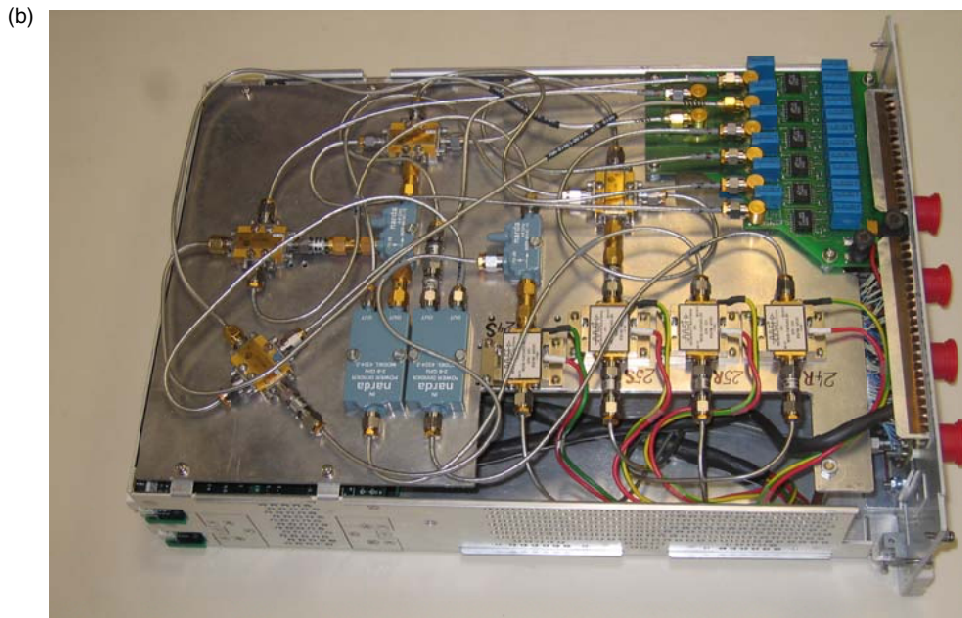
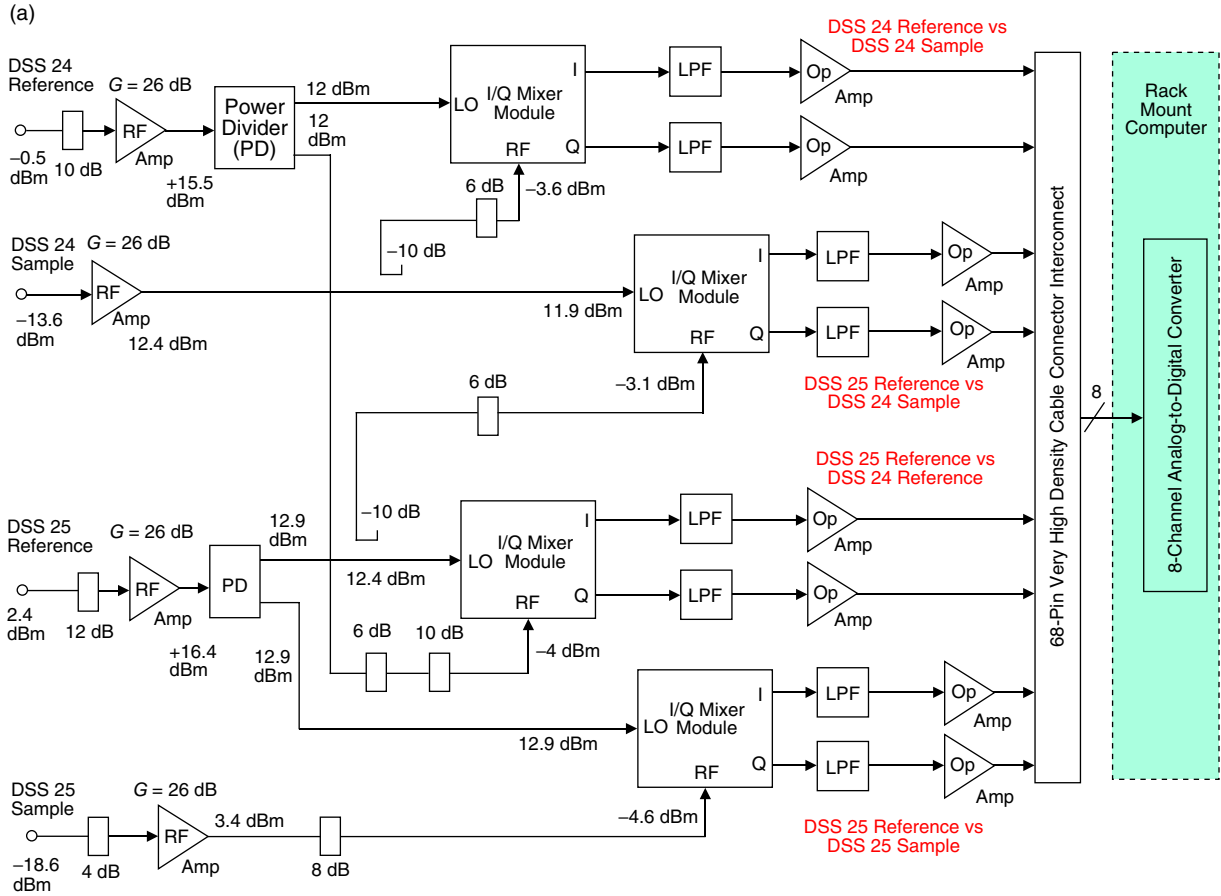


Fig. 2. Phase comparator assembly: (a) block diagram of the microwave electronics and (b) a picture of the completed PCA, showing the microwave components and inputs (used with permission of Spaceborne, Inc).

signals from two antennas (nominally Deep Space Station (DSS) 24 and DSS 25). The return signal path is green in Fig. 1. The PCA outputs consist of complex samples of equal magnitude representing the phase difference between the DSS 24 reference and sample, the DSS 25 reference and sample, the DSS 24 and DSS 25 references, and the DSS 25 reference compared to the DSS 24 sample.

The phase errors introduced in the PCA by radio frequency (RF) mixer phase imbalance and amplifier biases will be calibrated and compensated for by a Labview program after digital sampling. The PCA is designed to provide roughly 5-deg root-mean-square (rms) accuracy after calibration. The phase measurement accuracy was estimated based on analysis of component voltage standing wave ratio (VSWR) and phase imbalance, and will be verified by further testing. The power levels of the DSS 24 and DSS 25 reference and sample signals shown in Fig. 2(a) were measured at Goldstone using a transmitter setting of 10 kW, which is in the middle of the region of interest for our experiments (3 kW to 20 kW). A 100-Hz low-pass filter (LPF) is applied at baseband after the RF mixers to reduce noise and smooth out fluctuations. After amplification, the baseband signals are sampled by an 8-channel, 16-bit analog-to-digital converter. These samples are processed in Labview to remove any DC offsets, and the phase is computed by taking the arctangent of the in-phase (I) and quadrature-phase (Q) baseband signals.

The object of the phase measurement at SPC 10 is to estimate the phase of the signal, at some well-defined point such as the phase center, as it leaves the antenna. It is believed that the path length, and hence the phase, are stable within the beam waveguide in each antenna, between the PA output coupler and the phase center (see Fig. 1). Therefore, a measurement of the phase variations at the coupler output is sufficient to characterize the phase variations in the transmitted signal, after far-field phase calibration has been completed [1,2].

There are two distinct kinds of phase drift that need to be identified and treated separately: one-way and two-way phase drifts. One-way drift refers to phase effects in either the outgoing or the return signal, but not both. Two-way drift refers to phase effects occurring simultaneously in both the outgoing and return paths.

An example of one-way drift might be a phase change occurring in the PA, induced by increasing the transmitted power during an experiment (this effect has been noted in previous experiments). Direct measurement of the phase change at SPC 10 is sufficient to describe the change in phase of the signal leaving the antenna.

An example of two-way drift is the change in measured phase due to a temperature-induced change in the electrical length of the optical-fiber bundle. The phase measured at SPC 10 now includes phase changes in both the outgoing and return signals and, therefore, does not represent the phase of the signal leaving the antenna. If the two path lengths are the same, and change by the same amount due to thermal effects, then we can estimate the transmitted phase as half of the round-trip phase measured at SPC 10. If the outgoing and return path lengths are substantially different, then a different fraction, $0 < \alpha < 1$, should be applied to the measured phase; this problem requires further experimental and theoretical investigation.

During actual far-field uplink array calibration tracks, the transmitted frequencies are not constant, as assumed above, but rather change with time to compensate for Doppler. An example of the rate and magnitude of a realistic Doppler frequency trajectory is shown in Fig. 3. The cyclic variations are due to Mars orbit, while Earth rotation generates a much slower increase from one minimum to the next. Note that time intervals over which the frequency changes by a prescribed amount vary in duration over this nearly sinusoidal trajectory: when the rate of change is minimum, (T_1, T_3, T_5) , a relatively large amount of time is available for phase measurements, but during maximum rates of change, (T_2, T_4) , the available time becomes substantially less.

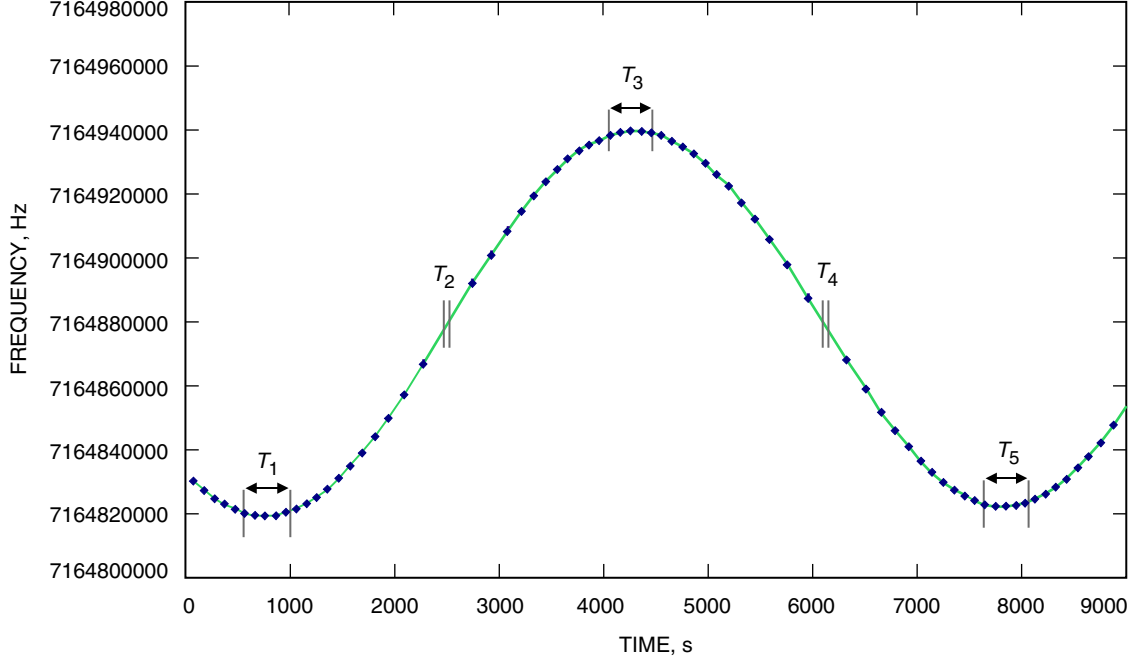


Fig. 3. Example of MGS uplink frequency trajectory, showing regions of nearly constant frequency due to Mars orbital dynamics.

III. Measurement of Electrical Phase at Different Frequencies

Phase measurements performed at different frequencies over long path lengths cannot be used to estimate phase drifts in the ground system directly, because a change in frequency itself induces a change in phase. This effect must be properly taken into account before meaningful estimates of ground system phase drift can be obtained. However, the additional phase due to the frequency difference can be estimated, if the electrical path length is known.

A. Electrical Distance Measurement

The following symbols will be used throughout this article in the mathematical model of the signal distribution system and phase measurement algorithms. The number of antennas in the uplink array is denoted by K ; the set of time-varying phases at each of the K antennas is $\{\theta_k(t)\}$; the set of distances from the control center to each of the K antennas is $\{d_k(t)\}$; the Doppler-shifted frequency, in hertz, for each antenna is $\{f_k(t)\}$; the wavelengths corresponding to the Doppler-shifted frequency at each antenna are denoted by $\{\lambda_k(t)\}$; n is the index of refraction of the fiber-optic cables; c_0 is the speed of light in a vacuum (299,792,458 meters per second); and c is the speed of light in a fiber-optic cable, reduced by a factor of n over the speed of light in vacuum.

The exact frequency of the transmitted X-band signal at antenna k is $f_k(t)$ at time t . The optical fibers used to link antennas to the control center have an index of refraction n ; hence, the speed of propagation in the fiber is $c = c_0/n$. Recalling the general relationship between speed, wavelength, and frequency, $c = \lambda_k(t)f_k(t)$, it follows that if the frequency varies with time then so does the wavelength:

$$\lambda_k(t) = \frac{c}{f_k(t)} \quad (1)$$

Assuming the round-trip light time is negligible, the number of wavelengths contained in a fiber-optic cable of length $d_k(t)$ at time t is

$$N_k(t) \equiv \frac{d_k(t)}{\lambda_k(t)} = \frac{d_k(t)f_k(t)}{c} \quad (2)$$

Note that $N_k(t)$ is not necessarily an integer, since $d_k(t)$ is in general an arbitrary multiple of the wavelength $\lambda_k(t)$. The absolute phase between the two cable ends can be defined as

$$\Theta_k(t) \equiv 2\pi N_k(t) = \frac{2\pi}{c}d_k(t)f_k(t) \quad (3)$$

This expression shows that absolute phase is proportional to frequency. If the absolute phase and exact frequency were available, and if in addition we assume that $d_k(t) = d_k$ is approximately constant over a suitably short time interval ($t_1 < t < t_2$) around time t , then the distance could be found by measuring the absolute phase and substituting into Eq. (3). Even if the absolute phase is not known, the change in absolute phase can be determined at two different times, t_1 and t_2 , using two different frequencies, $f_k(t_1), f_k(t_2)$. We can now solve Eq. (3) for d_k as follows:

$$d_k(t_1 < t < t_2) = \frac{c}{2\pi} \frac{\Theta_k(t_2) - \Theta_k(t_1)}{f_k(t_2) - f_k(t_1)} \cong \frac{c}{2\pi} \frac{\Delta\Theta_k(t)}{\Delta f_k(t)} \quad (4)$$

For the case of long fibers that contain a great many but unknown number of wavelengths, we typically do not have access to the absolute phase. Instead, we have access only to the measured phase, defined as

$$\theta_k(t) = 2\pi \frac{d_k(t) \bmod \lambda_k(t)}{\lambda_k(t)} \quad (5)$$

In Eq. (5), the term $d_k(t) \bmod \lambda_k(t)$ is the amount by which the electrical distance $d_k(t)$ is greater than the next lowest integer multiple of $\lambda_k(t)$. When that distance is divided by the wavelength $\lambda_k(t)$, the result is the fraction of a wavelength by which $d_k(t)$ exceeds an integral multiple of $\lambda_k(t)$. Multiplying this fraction by 2π , as in Eq. (5), yields the measured electrical phase in radians.

Next, the frequency and hence the wavelength, $\lambda_k(t)$, are varied in order to sweep $\theta_k(t)$ from 0 up to 2π . In principle, this can be done by starting with a frequency such that $\theta_k(t) = 0$. This frequency then can be increased in order to decrease the wavelength $\lambda_k(t)$, thereby sweeping $\theta_k(t)$ through 2π radians, or equivalently zero. Performing such a sweep gives us two values of $\lambda_k(t)$ such that $\theta_k(t) = 0$, establishing the electrical distance measurement. Setting the expression for phase at the start of the sweep, t_1 , to zero yields

$$\theta_k(t_1) = 2\pi \frac{d_k(t_1) \bmod \lambda_k(t_1)}{\lambda_k(t_1)} = 0 \quad (6)$$

At the end of the sweep, t_2 , after the frequency has been increased (or wavelength decreased), the expression for phase is again

$$\theta_k(t_2) = 2\pi \frac{d_k(t_2) \bmod \lambda_k(t_2)}{\lambda_k(t_2)} = 0 \quad (7)$$

Defining

$$M \equiv \frac{d_k(t_1)}{\lambda_k(t_1)} \quad (8)$$

where M is the integer number of wavelengths equal to the electrical distance at time t_1 , we can see that the number of wavelengths contained in the electrical distance $d_k(t)$ at t_2 must have increased by exactly one wavelength, whenever Eqs. (8) and (9) are satisfied:

$$M + 1 = \frac{d_k(t_2)}{\lambda_k(t_2)} \quad (9)$$

A similar argument applies for decreasing frequencies, but then we subtract 1 from M . Since the electrical distance $d_k(t)$ varies slowly with thermal changes, we can assume that it remains constant over the duration of the electrical distance measurement, $d_k(t) = d_k$. This allows us to rewrite Eqs. (8) and (9) as

$$M = \frac{d_k}{\lambda_k(t_1)} \quad (10)$$

$$M + 1 = \frac{d_k}{\lambda_k(t_2)}$$

Substituting for M and rearranging, we obtain

$$1 = \frac{d_k}{\lambda_k(t_2)} - \frac{d_k}{\lambda_k(t_1)} = d_k (\lambda_k^{-1}(t_2) - \lambda_k^{-1}(t_1)) \quad (11)$$

The electrical distance is found by solving equation Eq. (11) to obtain

$$d_k = (\lambda_k^{-1}(t_2) - \lambda_k^{-1}(t_1))^{-1} \quad (12)$$

The wavelengths $\lambda_k(t_1)$ at the start of the measurement and $\lambda_k(t_2)$ at the end of the measurement are found using Eq. (1). Substitution of Eq. (1) into Eq. (12) yields the electrical length in terms of the known frequencies at the beginning and end of the measurements:

$$d_k = (\lambda_k^{-1}(t_2) - \lambda_k^{-1}(t_1))^{-1} = c(f_k(t_2) - f_k(t_1))^{-1} \quad (13)$$

The procedure for determining the electrical distance by inducing a 2π radian phase change can be summarized as follows:

- (1) Perform a frequency sweep in which the frequency applied to antenna k is increased. A linear frequency ramp is well-suited for this purpose.
- (2) Note the time when the measured phase $\theta_k(t)$ of the return signal from antenna k is exactly zero, and call this time t_1 . We now have $\theta_k(t_1) = 0$.
- (3) As the frequency ramp continues, note the next time when $\theta_k(t)$ is zero, and call this time t_2 .
- (4) Using the known frequencies at times t_1 and t_2 , find the electrical distance using Eq. (13).

In uplink arraying applications, the quantity of interest is the real-time phase $\theta_k(t)$ so that variations due to thermal effects and equipment drift can be measured and corrected. In the above derivation, we have assumed that the speed of light in the optic fiber, c , was known. Although the speed of light in vacuum is known with great precision, the speed of light in the optic fiber depends on the index of refraction n , an approximate value that usually is obtained from the manufacturer's specification sheets but is not usually measured in the field. However, it is important to observe that, even if the true index of refraction of the fiber-optic cable, n , is unknown, the estimate of real-time phase $\theta_k(t)$ is not affected. This can be demonstrated by noting that for any frequency $f_k(t)$ we have

$$\lambda_k(t) = \frac{c}{f_k(t)} = \frac{c_0}{nf_k(t)} \quad (14)$$

where c_0 is the speed of light in vacuum. Equation (14) shows that $\lambda_k(t) \propto 1/n$. By Eq. (13), it is also true that $d_k \propto 1/n$ since $c = c_0/n$. The $1/n$ term cancels out in Eq. (7); therefore, the same value of $\theta_k(t)$ will be obtained regardless of n . This means that knowledge of the index of refraction is not necessary for the purpose of uplink array phasing where $\theta_k(t)$ is the quantity of interest.

B. Averaged Electrical Distance Measurement

The above procedure illustrates the concept of the electrical distance measurement, but it is only a single estimate of the electrical distance; hence, it may not be reliable in the presence of significant measurement errors. A more robust procedure for determining electrical distance counts a large number of phase cycles instead of a single cycle, in effect averaging out the error incurred during each measurement (assuming zero-mean measurement errors), hence reducing the error variance in proportion to the number of cycles.

With the cycle-averaging approach, the measurement is carried out over $P_k > 1$ cycles, since a large P_k would greatly reduce the error in the computed value of d_k . We also generalize the measurement somewhat by noting that it is not necessary to have $\theta_k(t_1) = 0$ at the start and $\theta_k(t_2) = 0$ at the end of the frequency ramp; we merely have to measure the *total* change in phase and in so doing determine both the integer number of cycles and the fractional-cycle remainder through which we have swept $\theta_k(t)$. Denoting the integer part of the phase change by P_k , and the fractional part by ΔP_k , we obtain

$$P_k + \Delta P_k = \frac{\theta_k(t_2) - \theta_k(t_1)}{2\pi} \quad (15)$$

where $\theta_k(t_2) - \theta_k(t_1)$ is the total phase change. Note that the number of cycles is also the number of extra wavelengths contained in the electrical distance d_k as the wavelength changes due to the frequency sweep. For example, if $\Delta\theta_k = 9\pi$, then the frequency sweep has shortened the wavelength so that 4.5 extra wavelengths are now contained in the distance d_k . We modify Eq. (11) to read

$$P_k + \Delta P_k = d_k (\lambda_k^{-1}(t_2) - \lambda_k^{-1}(t_1)) \quad (16)$$

The same change can be substituted in Eqs. (12) and (13) to obtain

$$d_k = (P_k + \Delta P_k) (\lambda_k^{-1}(t_2) - \lambda_k^{-1}(t_1))^{-1} = c(P_k + \Delta P_k) (f_k(t_2) - f_k(t_1))^{-1} \quad (17)$$

Equation (17) is more robust with respect to errors in the measurement of the starting and ending frequencies for large values of P_k . It is also robust with respect to errors in P_k itself. For example, if $P_k = 1$ and $\Delta P_k \cong 0$, then a measurement error of just 0.2 cycles will cause a 20 percent error in d_k .

If $P_k = 100$, however, then a measurement error of 0.2 cycles will cause only a 0.2 percent error in d_k . For this reason, measurement of phase over a large number of cycles is the preferred method. The following examples illustrate key points in the application of these techniques.

Example 1. Determination of Electrical Path Length. This example uses actual data obtained during an experiment to measure the round-trip electrical path lengths between SPC 10, DSS 24, and DSS 25. The return signal was coupled out after the power amplifier, as shown in Fig. 1. In this scenario, an uplink array consisting of two antennas will be used. We assume that the electrical distances are initially unknown. The first step is the determination of electrical distances d_1 and d_2 . Assume that a frequency ramp is applied to both antennas, with $f_1 = 7.150000$ GHz and $f_2 = 7.150240$ GHz. This is a frequency difference of 240 kHz. The total phase change measured at antenna 1 is $\Delta\theta_1 = 13285$ deg and that the total phase change measured at antenna 2 is $\Delta\theta_2 = 13469$ deg. This means that at antenna 1 the change in wavelength has caused a sweep through $P_1 + \Delta P_1 = 13285 \text{ deg}/360 \text{ deg} = 36 + 0.90278$ cycles. Likewise, the change in wavelength at antenna 2 has caused a sweep through $P_2 + \Delta P_2 = 13469 \text{ deg}/360 \text{ deg} = 37 + 0.41389$ cycles. Using Eq. (17), and assuming that $n = (0.72)^{-1}$ so that $c = 0.72c_0$ in the fiber-optic cables, we have

$$\begin{aligned} d_1 &= \frac{(0.72c_0)(36.90278)}{240 \text{ kHz}} \\ &= 3.319 \cdot 10^4 \text{ m} \\ &= 33.19 \text{ km} \end{aligned} \tag{18}$$

at antenna 1. A similar calculation yields 33.65 km at antenna 2. These numbers are consistent with the known physical distances from SPC 10 to the DSS 24 and DSS 25 antennas.

Example 2. A One-Millimeter Change in Distance with a Constant Frequency. Suppose that the carrier frequency remains constant at 7.0 GHz but that there is a 1-mm change in electrical path length. The absolute phase is given by

$$\Theta_k(t) \equiv 2\pi N_k(t) = \frac{2\pi}{c} d_k(t) f_k(t) \tag{19}$$

A change in electrical distance thus is given by

$$\Delta d_k = \frac{c\Delta\Theta}{2\pi f_k(t)} \tag{20}$$

Although we cannot measure absolute phase directly, the change in absolute phase is equal to the change in observable relative phase. This quantity can be measured, and Eq. (20) can be applied. A numerical example illustrating the measurement of a 1-mm change in electrical distance due to thermal expansion is shown in Table 1. A 1-mm change in total electrical distance thus results in a change of 8.4 deg in phase, which is measurable. The change in phase of the signal leaving the transmitter can be estimated by dividing this measured value by 2, yielding 4.2 deg as the final estimate.

Note that the importance of electrical distance lies in the phase change produced by changes in electrical distance. Hence, even though absolute electrical distance should be scaled by the index of refraction n , this effect cancels out when we are computing the quantity of interest, which is the phase effect caused by electrical distance. Hence, we use $n = 1$ in this and all other examples.

Table 1. Numerical example illustrating the phase change of 0.1467 rad caused by a 1-mm thermal expansion in electrical distance.

Time, s	Frequency, GHz	λ , m	Wavelengths	True distance, km	Δ frequency, Hz	Phase, rad	Δ phase, rad	Δ distance, m
0	7.0000000	0.042827494	700484.5999	30.00000000	—	3.769384146	—	—
1000	7.0000000	0.042827494	700484.6233	30.00000100	0	3.916093298	0.146709152	0.001

Changes in the electrical distance $d_k(t)$ must be measured over time since electrical distance is affected by the temperature of the fiber optics and other physical factors. Since $d_k(t)$ is assumed to be a slowly varying function of time, one can choose a time interval length T such that $d_k(t)$ is nearly constant from t to $(t + T)$ for all t . Since $d_k(t)$ is assumed to be nearly static over each interval, one can perform the following computation at each time interval:

$$d_k \left(nT + \frac{T}{2} \right) \approx \frac{c(\theta_k(nT + T) - \theta_k(nT))}{2\pi(f_k(nT + T) - f_k(nT))} \quad (21)$$

Frequency $f_k(t)$ and phase $\theta_k(t)$ are both assumed to be known at all times t . The slowly varying nature of $d_k(t)$ allows us to track electrical distance changes at the k th antenna by periodically evaluating Eq. (21). Continuous real-time phase measurements allow any phase-wrapping effects in $\theta_k(t)$ to be accounted for.

Example 3. Obtaining the Electrical Distance Under the Quasi-Static Assumption. An application of this method for $T = 10$ s is shown in Table 2. In Table 2, a frequency change of 50 kHz is applied over 10 s, a time during which the quasi-static assumption regarding electrical length certainly holds. The wavelength is seen to change by 306 nm. However, over a distance of 30 km, this produces more than 5 wavelengths of change, resulting in a phase rotation of over 31.437 rad in all. Substitution of the measured phase change and the measured frequency change into Eq. (21) yields a distance estimate of 30 km, which agrees entirely with the actual 30-km distance. Repeated applications of this measurement can be used to track changes in electrical distance over time.

Example 4. Measuring Electrical Distance Using Actual Mars Global Surveyor (MGS) Predicts. Referring to the realistic MGS predict frequency variations depicted in Fig. 3, we will determine the electrical distance at times (T_1, T_2, T_3) , which corresponds to a total change in Doppler frequency of approximately 80 kHz. We can use these available frequency variations themselves to generate a phase rotation at the PCA, thus enabling the estimation of electrical distance by means of Eq. (21). Since the rate of change of frequency is not at our disposal, the length of time T required for each measurement will necessarily be different at different times along the frequency trajectory, as indicated in Fig. 3. In this example, we assume that the round-trip electrical distance remains constant at exactly 30 km but that the MGS frequency predicts of Fig. 3 are used. Tables 3 through 5 illustrate these measurement concepts.

Example 5. Measuring Change in Electrical Distance at Different Frequencies. The change in phase from one epoch to the next can be inferred from the change in electrical distance caused by thermal effects (for example), using the relation $\overline{\theta_{\Delta d_k}} = 2\pi\overline{\Delta d_k}/\lambda$, where the overbar denotes the average of the wavelengths corresponding to the two epochs (the two end points of the measurement). Since a Doppler frequency of approximately 120 kHz is small compared to 7.15 GHz (their ratio is 1.68×10^{-5}), the true wavelengths at either end point could be used instead of the average, without incurring a significant

Table 2. Numerical example of distance measurement at two different times.

Time, s	Frequency, GHz	λ , m	True distance, km	Wavelengths	Δ frequency, Hz	Δ phase, rad	Estimated distance, km
0	7.000000000	0.042827494	30.000000000	700484.5999	—	—	—
10	7.000050000	0.042827188	30.000000000	700489.6034	50000	31.43767533	30

Table 3. Measured 30-km electrical distance near interval T_1 (Example 4). Measurement interval = 596 s (~ 10 min).

Time, s	Frequency, GHz	λ , m	True distance, km	Wavelengths	Δ frequency, Hz	Phase, rad	Δ phase	Estimated distance, km
757	7.164819428	0.041842291	30.000000000	716977.9529	—	5.987503064	—	—
1353	7.164827919	0.041842241	30.000000000	716978.8026	8490.666859	11.32603963	5.338536562	30

Table 4. Measured 30-km electrical distance near interval T_2 (Example 4). Measurement interval = 174 s (~ 3 min).

Time, s	Frequency, GHz	λ , m	True distance, km	Wavelengths	Δ frequency, Hz	Phase, rad	Δ phase	Estimated distance, km
2739	7.164892114	0.041841866	30.000000000	716985.2266	—	1.423515229	—	—
2913	7.164901053	0.041841814	30.000000000	716986.1211	8939.216531	7.044078969	5.62056374	30

Table 5. Measured 30-km electrical distance near interval T_3 (Example 4). Measurement interval = 594 s (~ 10 min).

Time, s	Frequency, GHz	λ , m	True distance, km	Wavelengths	Δ frequency, Hz	Phase, rad	Δ phase, rad	Estimated distance, km
3655	7.164930912	0.041841640	30.000000000	716989.109	—	0.684988005	—	—
4249	7.164939777	0.041841588	30.000000000	716989.9962	8865.617451	6.259276065	5.574288059	30

error. This example is similar to Example 4 in that it is assumed the distance d_k remains fixed within a measurement epoch (i.e., T_1), but it may change between epochs. Here it is assumed that the electrical path length changes by 1 mm between epochs, as does the frequency due to predicts; nevertheless, the change in path length is measured correctly using the frequency change at each epoch to generate the phase change.

As shown in Tables 6 through 8, a 1-mm change in the electrical distance can be detected with great accuracy at any frequency under the assumption that the electrical distance is quasi-static (i.e., static during the measurement interval). Therefore, this technique could be applied to monitor phase drifts

Table 6. Measured 30-km electrical distance near interval T_1 (Example 5). Measurement interval = 596 s (~ 10 min).

Time, s	Frequency, GHz	λ , m	True distance, km	Wavelengths	Δ frequency, Hz	Phase, rad	Δ phase, rad	Estimated distance, km
757	7.164819428	0.041842291	30.000000000	716977.9529	—	5.987503064	—	—
1353	7.164827919	0.041842241	30.000000000	716978.8026	8490.666859	11.32603963	5.338536562	30

Table 7. Measured 30-km electrical distance near interval T_2 (Example 5). Measurement interval = 174 s (~ 3 min).

Time, s	Frequency, GHz	λ , m	True distance, km	Wavelengths	Δ frequency, Hz	Phase, rad	Δ phase, rad	Estimated distance, km
2739	7.164892114	0.041841866	30.000001000	716985.2505	—	1.573680264	—	—
2913	7.164901053	0.041841814	30.000001000	716986.145	8939.216531	7.194244191	5.620563927	30.000001

Table 8. Measured 30-km electrical distance near interval T_3 (Example 5). Measurement interval = 594 s (~ 10 min).

Time, s	Frequency, GHz	λ , m	True distance, km	Wavelengths	Δ frequency, Hz	Phase, rad	Δ phase, rad	Estimated distance, km
3655	7.164930912	0.041841640	30.000002000	716989.1568	—	0.9853197	—	—
4249	7.164939777	0.041841588	30.000002000	716990.044	8865.61745	6.559608131	5.574288431	30.000002

by measuring the electrical distance, provided that a rapid frequency ramp can be applied each time a measurement is performed. The reason for the rapid frequency ramp is to minimize path length change during the measurement. In the next section, we relax this requirement by extending the above results to enable measuring the phase in the presence of simultaneous frequency and path length variations.

IV. Real-Time Monitoring of Local Phase

The following measurement technique does not assume constant electrical distance over the measurement interval, but does assume that a distance calibration has been performed using the frequency-ramp technique described in Section III.

Let times t_1 and t_2 be the start and end times of the measurement interval. The true change in phase, measured at SPC 10, is given by

$$\begin{aligned}
\Delta\theta_k &= 2\pi \left(\frac{d_k(t_2)}{\lambda_k(t_2)} - \frac{d_k(t_1)}{\lambda_k(t_1)} \right) \\
&= 2\pi \left(\frac{d_k(t_2)f_k(t_2)}{c} - \frac{d_k(t_1)f_k(t_1)}{c} \right) \\
&= \frac{2\pi}{c} (d_k(t_2)f_k(t_2) - d_k(t_1)f_k(t_1))
\end{aligned} \tag{22}$$

If a change in electrical distance and frequency occurs over the measurement interval, then we can write $f_k(t_2) = f_k(t_1) + \Delta f_k$, $d_k(t_2) = d_k(t_1) + \Delta d_k$, and rewrite Eq. (22) as

$$\begin{aligned}
\Delta\theta_k &= \frac{2\pi}{c} \{ [d_k(t_1) + \Delta d_k][f_k(t_1) + \Delta f_k] - d_k(t_1)f_k(t_1) \} \\
&= \frac{2\pi}{c} \{ d_k(t_1)f_k(t_1) + f_k(t_1)\Delta d_k + d_k(t_1)\Delta f_k + \Delta d_k\Delta f_k - d_k(t_1)f_k(t_1) \} \\
&= \frac{2\pi}{c} \{ f_k(t_1)\Delta d_k + d_k(t_1)\Delta f_k + \Delta d_k\Delta f_k \}
\end{aligned} \tag{23}$$

If $\Delta d_k = 0$, then Eq. (23) reduces to $\Delta\theta_k = (2\pi/c)d_k(t_1)\Delta f_k$ and can be used to measure $d_k(t_1)$ by purposely changing the frequency and noting the resulting phase change. Note that the time evolution of either the frequency or the distance is not important—only their change enters into Eq. (23).

Equation (23) is an exact expression for the measured round-trip phase difference resulting from simultaneous changes in frequency and electrical delay. It consists of three terms: the change in phase due to change in electrical distance at frequency $f(t_1)$; a change in phase due to change in frequency at the initial distance; and a term due to change in both frequency and change in distance. The third term can be ignored in uplink arraying applications, as the following example illustrates.

Supposing Δf is 120 kHz, the greatest change possible due to Mars orbital dynamics is shown in Fig. 3. Even if we assume that the electrical length changes by as much as 1 m, which is much greater than any anticipated length change over a 30-km round-trip distance, the resulting phase change due to the third term in Eq. (23) is only $2\pi\Delta d_k\Delta f_k/c = 6.2832 \times 1.2 \times 10^5/3 \times 10^8 = 2.5 \times 10^{-3}$ rad, or 0.14 deg. Clearly, this term can be neglected in our application.

The second term represents the change in phase due to change in frequency, at the electrical distance initially measured at t_1 . Since the frequency trajectory due to predicts is known, this term can be subtracted out in real time. We denote this term by $\xi_k(t)$, where again t refers to time elapsed after initial calibration at t_1 .

The first term represents the change in phase due to a change in distance, using only the frequency at t_1 . This is the phase-drift term we need to monitor and subtract out from the calibration term in order to keep the uplink array phased up for a long time. Accounting for the round-trip distance, we denote the phase term leaving the antenna as a fraction α of the first term: $\psi_k(t) = 2\pi\alpha f_k(t)\Delta d_k(t)/c$, where time is measured from t_1 . We therefore can express the equation used to monitor the phase due to electrical path length change as

$$\psi_k(t) = \alpha[\theta_k(t) - \xi_k(t)], \quad t > t_1 \tag{24}$$

In summary, a practical procedure for real-time tracking of phase due to thermally induced change in electrical distance is

- (1) Apply a fast ramp for a suitably short time, so that changes in electrical distance are insignificant during the measurement interval, and determine $d_k(t_1)$.
- (2) Continue monitoring the phase in real time, using Eq. (24).

If the phase change occurred in only the outgoing path, such as in the power amplifier section of the signal distribution system, then $\alpha = 1$ in Eq. (24). If the measured phase is the result of round-trip phase accumulation, as with thermal expansion of the optical fibers, then the appropriate value of α is closer to 1/2, but the exact value remains to be determined.

Example 6. Computation of Electrical Distance when Both Frequency and Distance Change over the Measurement Interval. We will compute the change in electrical distance using the technique of Eq. (24). We will assume a 1-mm change in electrical length and use the MGS predicts for the frequency from 757 s to 1353 s (on the time axis of Fig. 3). It is assumed that the initial distance has been obtained using the fast-ramp technique of Section III, followed by measurement of the total change in phase, and subtraction of the accumulated phase due to the change in frequency; the phase components are clearly shown in Table 9. Note that the computed change in electrical distance is almost exactly 1 mm, with very little error. This technique therefore can be applied in real time to continuously monitor local phase drifts caused by thermal expansion of the optical fibers or other equipment instabilities.

Table 9. Example of phase tracking, when both distance and frequency change over the measurement interval.

Time, s	Frequency, GHz	λ , m	True distance, km	Wavelengths	Phase, rad	Δ frequency, Hz	Phase change, rad	Δ , m	
757	7.164819428	0.041842291	30.000000000	716977.9529	5.987503064	—	—	—	
1353	7.164827919	0.041842241	30.000001000	716978.8265	11.47620331	8490.666859	5.48870	0.00100	
							$\Delta\theta$ (net)	5.48870	
							$\Delta\theta$ (frequency)	5.33854	
							Difference, rad	0.15016	
							Δ distance, m	0.00100	

V. Summary and Conclusions

In this article, a method for initially estimating electrical distance and continuously monitoring time-varying phase drifts has been presented. The technique uses the transmitted carrier signal itself as the reference; hence, it does not rely on an external reference frequency to provide a stable local oscillator. However, it does require accurate knowledge of the carrier frequency to enable removal of accumulated phase due to time-varying changes in transmitted frequency, such as occurs during Doppler compensation. This phase measurement technique does not inherently distinguish between round-trip and one-way phase effects; hence, the cause of the phase change has to be determined separately. Since the primary goal of round-trip phase measurement for uplink array applications is the estimation of the phase drift at the antenna phase center, it is important to distinguish between round-trip phase accumulation, for which approximately half of the measured phase applies, and phase drifts in the power amplifier section, all of which affects the antenna phase. In addition, this technique must be extended to include modulated carrier signals that will be encountered during actual uplink arraying operations.

References

- [1] V. Vilnrotter, R. Mukai, and D. Lee, “Uplink Array Calibration via Far-Field Power Maximization,” *The Interplanetary Network Progress Report*, vol. 42-164, Jet Propulsion Laboratory, Pasadena, California, pp. 1–16, February 15, 2006. http://ipnpr/progress_report/42-164/164D.pdf
- [2] V. Vilnrotter, D. Lee, T. Cornish, R. Mukai, and L. Paal, “Uplink Arraying Experiment with the Mars Global Surveyor Spacecraft,” *The Interplanetary Network Progress Report*, vol. 42-166, Jet Propulsion Laboratory, Pasadena, California, pp. 1–14, August 15, 2006. http://ipnpr/progress_report/42-166/166F.pdf